Chapter VIII

CURRENT AND NEW OBSERVING PROGRAMS FROM THE GROUND AND SPACE

https://doi.org/10.1017/S1743921313002913 Published online by Cambridge University Press

Solar and Astrophysical Dynamos and Magnetic Activity
Proceedings IAU Symposium No. 294, 2012
A.G. Kosovichev, E.M. de Gouveia Dal Pino, & Y. Yan, eds.

doi:10.1017/S1743921313002913

Observational methods for stellar magnetism: from detection to cartography

Klaus G. Strassmeier, Thorsten A. Carroll, Ilya Ilyin and Silva Järvinen

Leibniz-Institute for Astrophysics Potsdam (AIP)
An der Sternwarte 16, D-14482 Potsdam, Germany
email: kstrassmeier@aip.de, tcarroll@aip.de, ilyin@aip.de, sjarvinen@aip.de

Abstract. We review some of the currently used techniques to detect stellar magnetic fields on cool stars. Emphasis is put on spectropolarimetry with high-resolution spectrographs and its related data de-noising techniques and multi-line inverse modeling. Detections and results from Zeeman splittings and broadenings are briefly mentioned. We discuss some of our most recent Zeeman Doppler Imaging (ZDI) results and present a comparison of ZDI maps of the K-type WTTS V410 Tauri and the planet-hosting F8 star HD 179949 with results from other groups.

Keywords. Magnetic fields, polarization, stars: activity, stars: rotation, stars: spots, Sun: rotation, instrumentation: polarimeters, instrumentation: spectrographs

1. Why observing stellar magnetic fields?

One possible answer is that we should clarify more quantitatively whether magnetic fields influence stellar evolution or not and, if yes, how (see Mestel 2001). At least for low-mass stars there is the potential that stellar evolution theory must be rewritten to a certain extend if magnetic fields play a role. The best example is the "faint young Sun paradox" (Kasting & Grinspoon 1991). Some authors (Canuto *et al.* 1982, Wood *et al.* 2002, Spada *et al.* 2012) suggest that the Sun in its early years must have been an order of magnitude more magnetically active than today and then could have supported a young Earth and Mars with a much warmer climate. The Sun's magnetic activity and its corresponding proxies are expected to have declined steadily to today's levels as the solar rotation slowed due to magnetic braking (Skumanich 1972). However, classic stellar evolutionary models predict that the Sun was just 30% less luminous in its early main-sequence years than today, yet geological and biological evidence points to a much warmer young Earth than fully compatible with classical solar evolution models. Obviously, if we believe the 30% number, then the young Sun's extra output must have been non-thermal of origin. This is exactly what is observed for well-studied T Tauri and even ZAMS stars.

What exactly do we need to know for a more quantitative answer? Firstly, we must further refine the capabilities to observe stars as we observe the Sun, i.e., spatially resolve stellar surfaces using ZDI techniques with high-resolution spectrographs. Secondly, we must try to quantify the same type of laws that trace solar activity and solar magnetism (see, e.g., Strassmeier 2009). This includes stellar butterfly diagrams, Spörer's and Hale's laws, differential rotation and meridional circulation and, of course, the magnetic-field morphology and strength. Thirdly, all of these laws must mature to a quantitative level that bypass the current caveats for conclusive observational interpretation (e.g. the assumption of the weak-field approximation, simplified or even neglected radiative transfer in magnetized media, the use of only circular polarization and averaged line profiles).

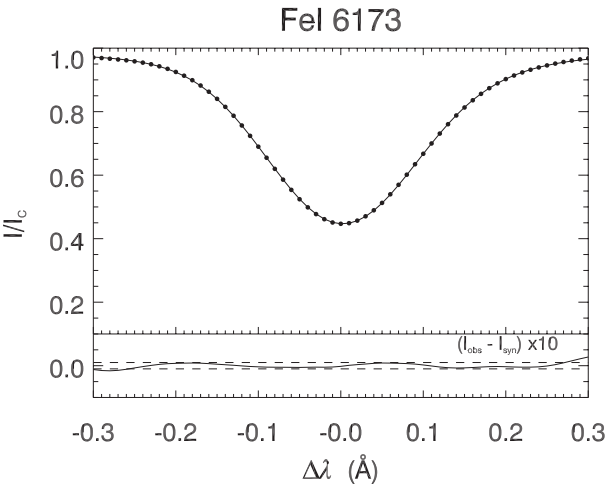

Figure 1. Inversion fit to an averaged line profile of HD 123351. Shown is the PCA-enhanced average profile from 273 individual Zeeman-sensitive Fe I 6173 line profile (dots). The line is the inversion fit with a total of six free parameters. Note that the average effective temperature came out to 4830 K with a peak-to-valley variation of 60 K due to spots. The inferred magnetic flux density was 542 G with a formal error of 72 G and a peak-to-valley amplitude of about 80 G. The lower panel shows the residuals enhanced by a factor of ten.

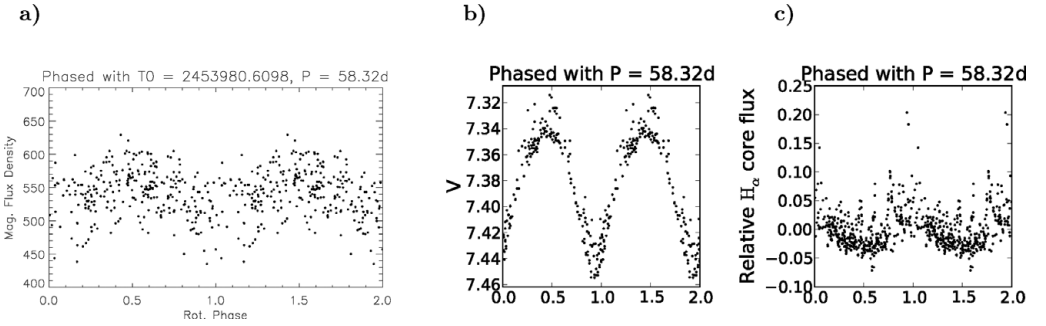

Figure 2. Magnetic-flux density variation of the active star HD 123351 ($P_{\rm rot}$=58.32 d, $v \sin i$=1.8±0.7 km s^{-1}). *a.* A plot of all individual 273 flux-density measurements versus rotational phase. *b.* The simultaneous photospheric V-band light curve. *c.* The simultaneous chromospheric Hα-core flux. Note the phase coherence of $f.B$ with the photospheric light and the anti-phase coherence with the chromospheric emissions.

2. Detections from Zeeman broadening and spectropolarimetry

2.1. *Zeeman splittings and broadenings*

Its basis is the splitting of a spectral line into a linearly polarized but unshifted π component and two circularly polarized σ components whose separation $\pi \pm \sigma$ is proportional to B, λ^2, and the effective Landé factor g of the transition. Zeeman splitting outside a lab was first noticed in a spectrum of a sunspot (Hale 1908). As we know, it was the discovery of the very first, extraterrestrial, magnetic field (see IAU Symp. 273). The very same technique but with refined atomic line lists, larger wavelength ranges and multi-line approaches, more appropriate radiative-transfer treatment and, of course, higher spectral resolution and signal-to-noise ratio (S/N) to minimize blending has been subsequently applied to other stars. Reviews of the historical development can be found in, e.g., Valenti *et al.* (1995), Johns-Krull *et al.* (2008), Donati & Landstreet (2009).

https://doi.org/10.1017/S1743921313002913 Published online by Cambridge University Press

Full Zeeman line splitting is rarely observed and requires very high spectral resolution, favorable near-IR lines, and few kG field strengths. An impressive splitting detection has been shown for AD Leo for the Ti I 2.23 μm line by S. Saar (priv. commun.). Typically, it is just the excess broadening of magnetically sensitive spectral lines with respect to insensitive lines that is observed. Mathys & Solanki (1989) originally followed a method suggested by Stenflo & Lindegren (1977) that introduced a statistical analysis of a large number of spectral lines based on line width measurements at different levels in the line profile in order to reduce the effects of blends. However, to differentiate the small excess line-broadening caused by a surface magnetic field from other line-broadening mechanisms such as thermal effects, micro- and macroturbulence or atomic line parameter variation, e.g. of the oscillator strengths, we need to use a more sophisticated line-profile inversion technique. Examples of such inversion techniques based on radiative transfer in magnetic atmospheres and its application to active cool stars can be found in, e.g., Saar (1988), Valenti *et al.* (1995), Ruedi *et al.* (1997), and Anderson *et al.* (2010). The Zeeman broadening of molecular FeH lines had been noticed in the NSO solar spectrum atlas (Wallace *et al.* 1998), and been used to detect magnetic fields on very cool stars (Berdyugina *et al.* 2003, Reiners & Basri 2006). However, even if all of above obstacles – tiny splitting, intrinsic line broadening, line blending, poor line lists – can be overcome one is left with the disentangling of the relative area covered with magnetic fields (the filling factor f) and of the average field strength B within this area. As noted by Johns-Krull *et al.* (2008), assuming a single field strength usually does not fit the line profiles properly and one needs to solve for the filling factor for a series of field strengths (and preferably also different lines). The product of the intensity-weighted mean magnetic field strength over the stellar disk and the respective filling factor is then the resulting average magnetic field density.

Usually, a single high-resolution spectrum provides too low a S/N for a direct magnetic analysis. One way to compensate this is by having many time-sampled spectra, e.g. obtained by using a robotic telescope. Time sampling of individual spectral line profiles can then be used, e.g. in a principal component analysis (PCA), to boost the S/N of a particular line by a factor of more than five (Fig. 1). It even allows to search for phase-dependent variations in Zeeman-sensitive spectral line profiles. This approach was applied to the active binary star HD 123351 (Strassmeier *et al.* 2011). A modulation of the magnetic flux density with the rotation period of the star was detected (Fig. 2a). Quite interestingly, the flux density varied in-phase with the photospheric light variability (Fig. 2b) and in anti-phase with the chromospheric emissions from Ca II H&K, He I D3, and Hα (the latter is shown in Fig. 2c). The measured magnetic flux likely stems not only from cool photospheric spots but also from bright plage-like regions. The magnetic field that is measured in $f.B$ then originates from a mixture of bright plage-like regions and dark spots, both with different respective filling factors, further complicating the detection.

2.2. *Spectropolarimetry: the quest for a signal*

For most (active) cool stars the typical signal amplitude of a single polarized line profile is of the order of a few times 10^{-4} relative to the normalized continuum. These values are far below the S/N ratio of a typical spectropolarimetric observation, which hardly exceeds 1,000:1. So the individual polarimetric line profiles are buried well below the noise level by typically one order of magnitude. This requires techniques that are able to recover and extract the line profile signals from the measurement noise prior to the actual ZDI analysis. Most of the techniques for circularized, i.e. Stokes V, line profiles

https://doi.org/10.1017/S1743921313002913 Published online by Cambridge University Press

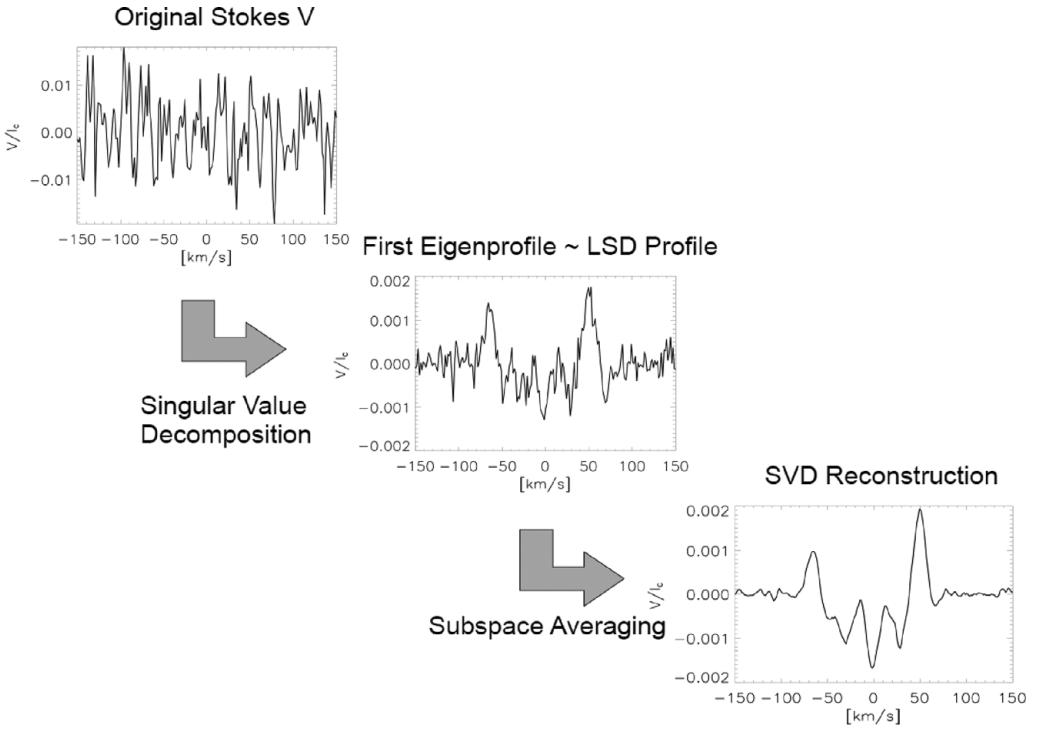

Figure 3. The two-step process of the "sub-space reconstruction method" (SSRM). Top left shows the original Stokes-V observation (shown is a small range around the Fe I 6173-Å spectral line). The first step is a singular value decomposition (SVD) of the original observation matrix. The next step uses the reduced-rank estimation of the covariance matrix to perform a coherent addition of the projection coefficients in signal subspace (SVD reconstruction).

take advantage of the fact that the polarized Stokes V patterns for almost all Zeeman sensitive atomic spectral lines are similar except for a non-linear scaling.

One popular extraction technique is the so called Least Squares Deconvolution (LSD; Donati *et al.* 1997). Under the assumption of the weak-field approximation, line profile shapes can be considered as equal and amplitudes are only linearly dependent upon their individual Landé factors and line strengths. The entire spectrum can be described as a sum of scaled and shifted identical profiles that can be de-convolved to create an average profile in velocity space. An improved version of LSD, called iLSD, was presented just recently by Kochukhov *et al.* (2010). These authors found that the Stokes LSD profiles do not behave as a real spectral line with respect to magnetic field and elemental abundance. This problem is especially prominent for the Stokes I variation with abundance and Stokes Q variation with magnetic field. Kochukhov *et al.* (2010) concluded that the usual method of interpreting the LSD profiles by assuming that they are equivalent to a real spectral line gives satisfactory results only in a limited parameter range. Another method for Stokes profile extraction is PCA (Carroll *et al.* 2007, Martínez González *et al.* 2008) where a multi-line PCA is used to reconstruct and de-noise individual Stokes profiles from a large number of observed profiles. Over LSD, this method has the great advantage that it facilitates a detailed radiative transfer based line-profile fitting. A more simple but also very effective coherent addition of line profiles in the velocity or logarithmic wavelength domain was put forward by Semel *et al.* (2009) and Ramírez Vélez *et al.* (2010).

https://doi.org/10.1017/S1743921313002913 Published online by Cambridge University Press

Järvinen & Berdyugina (2010) showed that the Occamian inversion can overcome the limitations of the classical two-temperature approximation (spot and photosphere), which was previously employed to LSD profiles, and to obtain true temperature maps based on stellar atmosphere models. The resulting maps agreed well with those obtained using their inversion code without LSD, provided the data are noiseless. The authors recommend to use LSD only for poor S/N data. Further, they showed that the Occamian inversion, both with and without LSD, reconstructs the surface temperature distribution reasonably well for an adequate spatial resolution, which means that the resulting map depends on the rotational line broadening. For instance, in a slowly rotating star, closely situated spots are usually recovered blurred and unresolved, which affects the obtained temperature range of the map.

Sennhauser & Berdyugina (2010) presented a method they called Zeeman Component Decomposition (ZCD) for recovering an intrinsic line profile and the mean longitudinal magnetic field from polarized spectra. ZCD can be deployed with minor prior information on the stellar parameters by fitting each atomic/molecular line depth independently and thus take out some of the profile nonlinearities due to blending. A comparison of first results with results from Grunhut *et al.* (2010) based on LSD showed that ZCD magnetic-field strengths were generally a factor of two smaller than from LSD. This was attributed by Sennhauser & Berdyugina (2011) to LSD being more prone to line blending than ZCD.

A new two-step Ansatz was devised just recently by Carroll *et al.* (2012) in their application to V410 Tauri; we call it the *subspace reconstruction method* (SSRM) which is based on a singular eigenvalue decomposition (SVD) of the observational matrix (see Fig. 3). From a large set of suitable and Zeeman-sensitive spectral line profiles (currently only Stokes V) an observation matrix in velocity domain is built. To search for systematic and correlated features common to all Stokes V profiles, a SVD analysis is applied to the observation matrix. The decomposition into eigenprofiles of the observation covariance matrix provides an efficient method for separating coherent and systematic structures present in all line profiles and non-coherent random features, e.g. noise and blends. The number of significant eigenprofiles determines the signal subspace (the reduced rank of the observation covariance matrix) that carries the majority of the profile information. In a second stage, which provides the actual signal boosting effect, a signal averaging in subspace is performed. This is done by projecting all Stokes V line profiles onto the limited number of eigenprofiles (dimensions) and eventually averaging over the projection coefficients. The effect of this two-stage process is – besides the actual signal extraction – a better noise suppression compared to conventional line profile averaging or LSD.

2.3. *Some recent results*

The morphology of the magnetic fields detected in single red giants by Konstantinova-Antova *et al.* (2008, 2009, 2012) suggest that these are likely due to a solar-type $\alpha\Omega$ dynamo. Application of the first-order moment technique led to a detection of a longitudinal field of $|B_l| \approx 10\,\mathrm{G}$ on the surface of the single giant V390 Aur based on LSD profiles. A ZDI map from the same Stokes-V data reconstructed peak magnetic field strengths of $+60\,\mathrm{G}$ to $-60\,\mathrm{G}$ for the radial component and somewhat less, $\pm 40\,\mathrm{G}$, for the azimuthal component and $+20\,\mathrm{G}$ to $-60\,\mathrm{G}$ for the meridional component. Different to another single G giant, HR 1362 (EK Eri; Dall *et al.* 2010), there appears to be no obvious dipolar preference for V390 Aur. Auriére *et al.* (2011) had obtained a ZDI map of EK Eri and found a pronounced dipolar structure. However, EK Eri is believed to be a descendant of a magnetic Ap/Bp star when it was on the main sequence and thus its field may be purely fossil.

https://doi.org/10.1017/S1743921313002913 Published online by Cambridge University Press

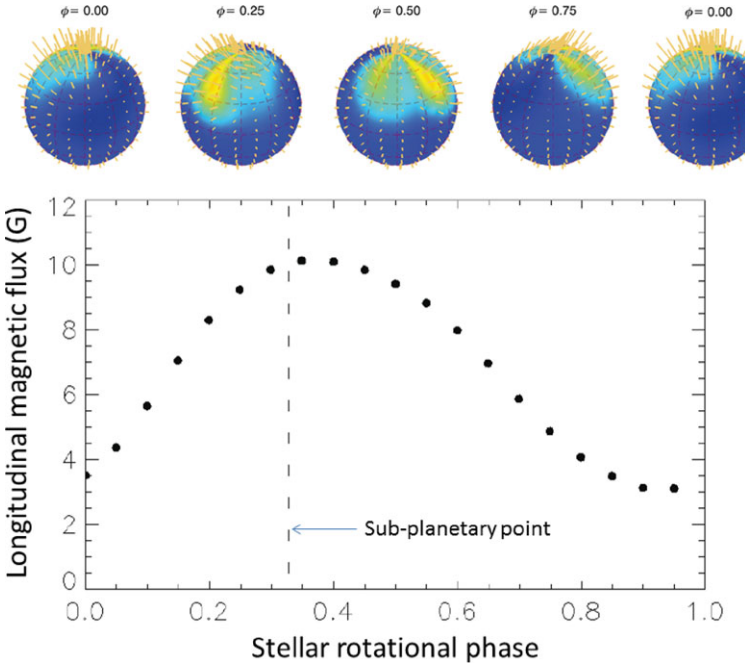

Figure 4. Longitudinal magnetic flux versus stellar rotation in the planet-hosting star HD 179949. The top row shows our preliminary ZDI maps at four rotational phases. The plot below shows the longitudinal magnetic flux in Gauss in 2011 versus the 7.6-d stellar rotation. The highest magnetic flux is seen around a phase when the sub-planetary point crosses the stellar central meridian. This suggests that there likely is a magnetospheric interaction between the planet and the star.

Sennhauser & Berdyugina (2011) announced the discovery of a magnetic field on Arcturus (K1.5III) from CFHT/Espadons data. For the two ZCD spectra, they reported an extremely weak longitudinal magnetic field of 0.65±0.26 G and 0.43±0.16 G. Such a weak field could be attributed to a diminishing $\alpha\Omega$-dynamo driven by convection and differential rotation in the deepening convection zone of the star. In the same paper, the authors applied ZCD also to Stokes-V spectra of 32 Cyg (K3Ib+) and λ Vel (K4.5Ib-II) and compared their results with previous LSD results from Grunhut *et al.* (2010). A line-of-sight component for 32 Cyg of 1.16±0.49 G from LSD and 0.53±0.16 G from ZCD was obtained, detto for λ Vel of 1.72±0.33 G and 0.90±0.13 G, respectively.

Zeeman signatures were detected on the M supergiant Betelgeuse (Auriére *et al.* 2010, Petit *et al.* 2013) corresponding to a longitudinal component of about 1 G. Time-series Stokes-V spectra unveiled a smooth increase of the longitudinal field from 0.5 to 1.5 G within approximately two months and were correlated with radial velocity fluctuations. This magnetic field may be associated to the giant convection cells that could enable a "local dynamo" rather than a solar-like $\alpha\Omega$ dynamo.

Fares *et al.* (2012) presented two magnetic maps for the Jupiter-hosting F8V star HD 179949 from data taken in 2007 and 2009. The star was previously reported to show enhanced Ca II H&K emission modulated by the orbital period of the planet† with a phase lag of ≈65° (Shkolnik *et al.* 2008). The reconstructed field from LSD profiles is rather weak (few G) and large scale with a mainly poloidal structure. No clear modulation with the planet's orbital period or the beat period between the stellar rotation and the

† The planet has a 3.1-d orbital period and is non eclipsing.

https://doi.org/10.1017/S1743921313002913 Published online by Cambridge University Press

orbital period was detected. Given the $v \sin i$ of just 7 km s^{-1}, a stellar rotation period of 7.6 d and a moderately-high spectral resolution of R=65,000, the surface is not or at most barely resolved. An independent set of higher resolution data was obtained by us with ESO/HARPS (R=115,000) and its new polarimeter in July 2011. The application of a variant of *iMap*, tailored to minimize the effects of phase gaps, led to a ZDI map with a dipolar-like magnetic feature of strength ≈10 G, quite comparable to the features in the Fares *et al.* (2012) 2009 map. The longitudinal magnetic flux appears strongest around the sub-planetary point (Fig. 4; shown with the dashed line in the plot). This preliminary result agrees with the simplest model where a magnetic interaction – if it exists – would be best visible when the planet is in front of the star.

3. Stellar surface cartography with Zeeman Doppler Imaging

3.1. *Improved polarized radiative transfer analysis*

Our basic platform for field cartography is the ZDI code *iMap* (Carroll *et al.* 2007, 2012) which simultaneously reconstructs the magnetic field and the temperature distribution from phase-resolved Stokes spectra. This code is versatile and flexible enough to be also applicable to Zeeman-broadened Stokes I profiles to perform the desired magnetic flux density inversion for the magnetic flux ($f.B$). In the past, there were two major obstacles that hampered a full polarized radiative transfer driven approach to ZDI. Firstly, the expected Stokes profiles are heavily contaminated by noise, or even buried within the noise, which makes their reliable analysis and interpretation difficult. Secondly, the radiative transfer calculation presents an enormous computational burden for the inverse problem where for each iteration and each surface segment the full radiative transfer equation has to be solved.

Approaches to tackle the first problem were summarized in Sect. 2.2. A possible solution for the second problem was introduced by Carroll *et al.* (2008) where an artificial neural network is used to solve the polarized radiative transfer and calculate individual Stokes lines profiles. The approach uses Multi-Layer-Perceptrons (MLPs) to approximate the mapping between the atmospheric parameters and the resulting Stokes spectra. The data base of local line profiles is first decomposed via PCA for the purpose of dimensionality reduction. Then, a set of MLP's is trained to calculate projection coefficients as a function of the five parameters $T_{\rm eff}$, magnetic-field strength, inclination and azimuth, and line-of-sight angle. The number of principal components of 10 is chosen in such a way that a direct reproduction of the Stokes profiles leads to an overall error of less than 10^{-4}. Once the MLP's have found a good approximation of the underlying functional dependence, they allow an impressively fast Stokes profile evaluation (a factor 1,000 faster compared to the conventional radiative-transfer calculation with DELO).

3.2. *Inverse multi-line modeling*

In Doppler imaging it is typical to use a combined long spectral line vector such that the error function, E, reads

$$E = \frac{1}{2} \sum_{p=1}^{N_p} \sum_{k=1}^{N_k} \sum_{m=1}^{N_m} (O_{\rm p,k,m} - I(x)_{\rm p,k,m})^2, \tag{3.1}$$

where x is the model parameter vector, p the rotational phase, k the spectral line, m the wavelength or the velocity index, and N_p, N_k, N_m their respective total numbers. This is the set up also for temperature DI with *TempMap* (e.g. Rice & Strassmeier 2000; Rice *et al.* 2011) but fails for ZDI due to the large noise and the increased parameter space.

https://doi.org/10.1017/S1743921313002913 Published online by Cambridge University Press

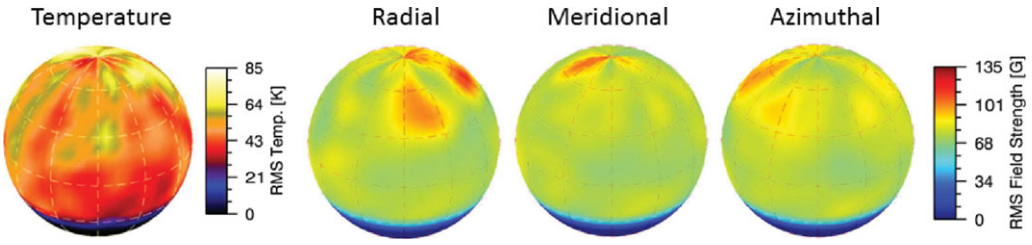

Figure 5. Error maps from a multi-line inversion of CFHT/Espadons data of V410 Tau ($V \approx$11.5 mag) with *iMap*. Left: errors of the temperature map; right: errors of the respective magnetic-component maps. Note the correspondence of the magnetic-field errors with the temperature.

It demonstrates that the reduced χ^2 as a measure of the goodness-of-fit is sometimes of limited use.

Another improvement in the *iMap* code is its new inversion module. While the former versions relied on a conjugate gradient method with a local entropy regularization, the current version of *iMap* uses an iteratively regularized Landweber method (Engl *et al.* 1996). Iterative regularization for inverse problems has been the subject of various theoretical investigations over the recent years (see references in Carroll *et al.* 2012). The Landweber iteration rests on the idea of a simple fixed-point iteration derived from minimizing the sum of the squared errors. Our new inversion routine follows exactly this line of argumentation. It deals with four parameter spaces (temperature, radial magnetic field, azimuthal magnetic field and meridional magnetic field) each of which with a dimension equal to the number of surface segments. The inversion algorithm has to navigate through the combined parameter space to find a solution that is compatible with the data. In order to study the stability of the inversion we use a simulation that runs the inversion with the original data set but from randomly chosen starting positions. Each of the four parameter spaces is independently initialized by choosing a random value for each surface segment. This led to the spatial error maps shown in Fig. 5. What can be seen from these maps is that the error values are correlated with the field strength as well as with the temperature. For V410 Tau a temperature change of just 80 K in a spotted region causes a change in the amplitude of the Stokes V signal of 4%. In the strong field regime of the polar spot this difference in amplitude is equivalent to a magnetic field of 60 G. This emphasizes once more the influence of the temperature on the magnetic field determination and leaves the frightening possibility that magnetic maps where the temperature was not included to be simply wrong.

3.3. *A recent application to V410 Tauri*

V410 Tauri is a weak-lined T Tauri stars that is dubbed a "young Sun". The ZDI magnetic field structures obtained recently by Carroll *et al.* (2012) show a good spatial correlation with the surface temperature and are dominated by a strong field within the cool polar spot (Fig. 6). Earlier, Rice *et al.* (2011) presented temperature maps from atomic and molecular lines from the same data. The ZDI maps exhibit a large-scale organization of both polarities around the polar cap in the form of a twisted bipolar structure. The magnetic field reaches a value of 1.9 kG within the polar region but smaller fields are also present down to lower latitudes. Within the polar spot the two polarities appear separated by a sharp, pole-crossing, neutral sheet. In total the field forms an S-shaped structure centered at the rotation pole. The topology is predominantly radial but 1 kG meridional components coexist very close to the pole. An azimuthal component, on the other hand, is restricted to certain regions and also reaches 1 kG at one point while the

https://doi.org/10.1017/S1743921313002913 Published online by Cambridge University Press

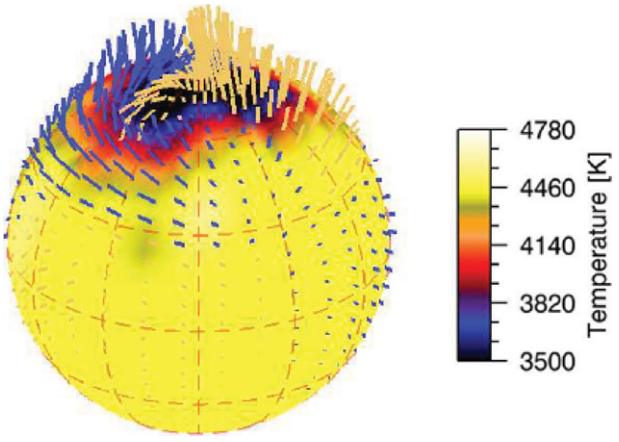

Figure 6. *iMap* ZDI of V410 Tau from SSRM line profiles and an iterative regularization. The magnetic field map is overlaid onto the (color coded) temperature map. Dark means cool. In a b/w presentation the darker field lines are of negative polarity (actually plotted in blue) and the brighter field lines are of positive polarity (in yellowish). The length of the vectors are proportional to the field strength of up to ±1.9 kG. The map is shown at rotational phase 0.00.

rest of it mostly remains near 500 G. Expressed in terms of the poloidal and toroidal components, we found that 73% of the surface field is poloidal and just 27% is toroidal. The pronounced non-axisymmetric field structure and the non-detection of a differential rotation for V410 Tau ($d\Omega = 0.007 \pm 0.009$) supports the idea of an underlying $\alpha^2\Omega$-type dynamo, which is predicted for weak-lined T Tauri stars. Following Küker & Rüdiger (1999) for an $\alpha^2\Omega$-dynamo the field topology at the surface can be expected to be non-axisymmetric with a typical S1- or A1-type geometry and appears to be in excellent agreement with the ZDI map.

In Fig. 7, we compare the magnetic map from *iMap* with the independent ZDI map of Skelly *et al.* (2010), based on the code by Brown *et al.* (1991). The eye immediately catches some significant differences†. Skelly *et al.* (2010) found that 50% of the total field has a toroidal component and the other 50% are poloidal and that the majority of the field shows strongly inclined large-scale azimuthal fields which are distributed over one entire hemisphere, whereas our reconstructed topology has only 27% toroidal fields and 73% poloidal fields with a strong radial and bipolar component around the polar region. In contrast to our reconstructed map where the strong magnetic fields are well correlated with the temperature, the fields of Skelly *et al.* (2010) seem to show almost no correlation with their brightness maps, i.e. a proxy of the temperature distribution. We note that our data were taken with CFHT/Espadons during December 5, 2008 to January 14, 2009. The fact that the Skelly *et al.* data were observed at almost the same time as ours at the Telescope Bernard Lyot with the *Narval* spectropolarimeter (January 2 to January 17, 2009), is certainly a reason for a closer inspection and comparison of the two results. We can only speculate about the reasons for the disparity of the two reconstructions but we want to emphasize that in contrast to Skelly *et al.* (2010) our approach makes no assumptions on the surface topology in terms of a spherical harmonic decomposition or potential field structure. It is furthermore fully based on polarized radiative transfer and line profile modeling instead of assuming a Gaussian local line profile and it pursues a

† The reader may beware of the slight difference of the two plot styles in Fig. 7, a so-called mashed polar view; the Skelly *et al.* map is shown for the entire surface while the Carroll *et al.* map is shown just down to the stellar equator.

https://doi.org/10.1017/S1743921313002913 Published online by Cambridge University Press

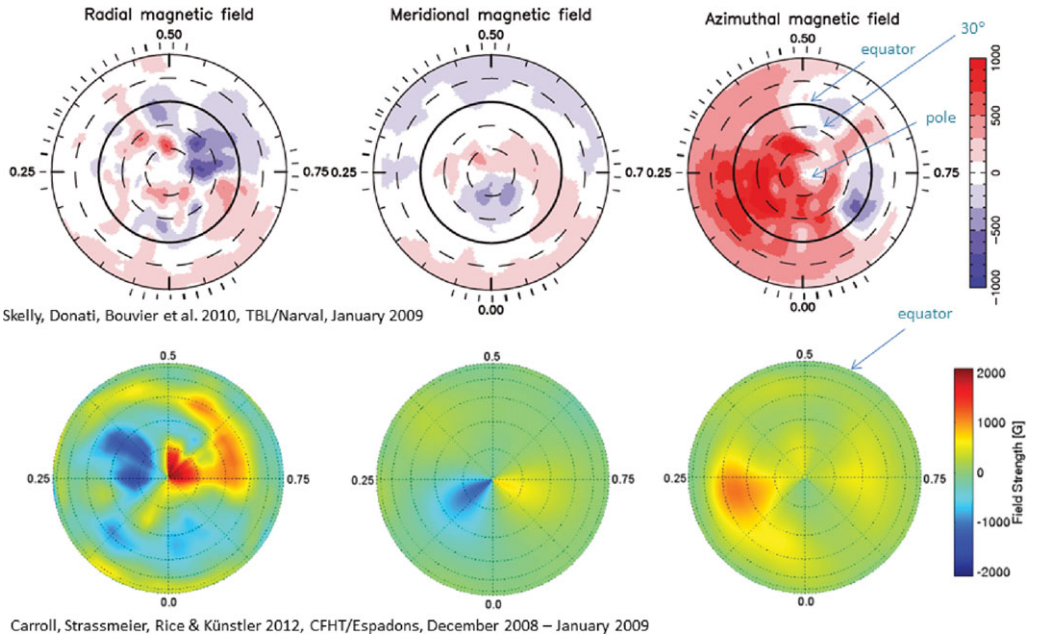

Figure 7. A comparison of two independent ZDI maps of the WTTS V410 Tauri. *Top row:* Skelly *et al.* (2010) map based on observations with TBL/Narval in the period of January 2009 and the Brown *et al.* (1991) code. *Lower panel:* Carroll *et al.* (2012) map based on observations with CFHT/Espadons in the period of December-January 2009 and the *iMap* code. The *iMap* ZDI is from Stokes V&I and SSRM, the Skelly *et al.* ZDI is from Stokes V alone and LSD. Note that the Skelly *et al.* map is shown for the entire surface while the Carroll *et al.* map is shown just down to the stellar equator.

strategy which simultaneously invert the temperature and magnetic field. This gives us enough confidence to believe in the validity of our new *iMap* results.

4. Summary

Polarimetry with high-resolution spectrographs makes it possible to reconstruct the detailed stellar surface magnetic field from time-series observations. More and more complex field topologies and/or smaller and smaller field strengths are detected, even if we only have circularly polarized information through the Stokes-V component yet. Promising first detections of linear line polarization were already announced for some bright late-type stars (Kochukhov *et al.* 2011). Future application to cool stars with even larger telescope apertures will incorporate the linearly polarized Stokes components also into ZDI but, as is the case today with Stokes-V, will run into sub-noise structure. At this point, we emphasize that high-quality CFHT/Espadons observations of a 11.5-mag K star return a sub-noise S/N ratio of 1:5 in Stokes-V (rather than 5:1 as one would already call a "low S/N ratio"). Very sophisticated data-handling and analysis tools are clearly mandatory. More developments in this direction are expected despite that future telescopes will have more light-collecting power. The upcoming PEPSI spectropolarimeter at the LBT (Ilyin *et al.* 2011) will make use of the entire 110 m^2 light-collecting surface of its two 8.4 m mirrors. This is almost ten times the light-collecting power of the 3.6m CFHT. And even it will be dwarfed by yet another factor of ten by the proposed spectropolarimeter for the HIRES spectrograph for the E-ELT (e.g. Strassmeier 2011). Let the good times roll.

https://doi.org/10.1017/S1743921313002913 Published online by Cambridge University Press

Acknowledgements

KGS likes to thank the organizers for the invitation to speak.

References

Anderson, R. I., Reiners, A., & Solanki, S. K. 2010, *A&A* 522, A81
Auriére, M., Donati, J.-F., Konstantinova-Antova, R., Perrin, G., Petit, P., & Roudier, T. 2010, *A&A* 516, L2
Auriére, M., Konstantinova-Antova, R., Petit, P., *et al.* 2011, *A&A* 534, A139
Berdyugina, S. V., Solanki, S. K., & Frutiger, C. 2003, *A&A* 412, 513
Brown, S. F., Donati, J.-F., Rees, D. E., & Semel, M. 1991, *A&A* 250, 463
Canuto, V. M., *et al.* 1982, Nature 296, 816
Carroll, T. A., Kopf, M., Ilyin, I., & Strassmeier, K. G. 2007, AN 328, 1043
Carroll, T. A., Kopf, M., & Strassmeier, K. G. 2008, *A&A* 488, 781
Carroll, T. A., Strassmeier, K. G., Rice, J. B., & Künstler, A. 2012, *A&A*, in press
Dall, T. H., Bruntt, H., Stello, D., & Strassmeier, K. G. 2010. *A&A* 514, A25
Donati, J.-F. *et al.* 1997, *MNRAS* 291, 658
Donati, J.-F. & Landstreet, J. 2009, *ARA&A* 47, 333
Engl, H. W., Hanke, M., & Neubauer, A. 1996, *Regularization of Inverse problems, Mathematics and Its application*, Kluwer Academic Publishers, Dordrecht, The Netherlands
Fares, R., Donati, J.-F., Moutou, C. *et al.* 2012, *MNRAS* 423, 1006
Grunhut, J. H., Wade, G. A., Hanes, D. A., & Alecian, E. 2010, *MNRAS* 408, 2290
Hale, G. E. 1908, *ApJ* 28, 315
Ilyin, I., Strassmeier, K. G., Woche, M., Dionies, F., & Di Varano, I. 2011, *AN* 332, 753
Järvinen, S. & Berdyugina, S. V. 2010, *A&A* 521, A86
Johns-Krull, C. M. 2008, in *14th Cambridge Workshop on Cool Stars, Stellar Systems, and the Sun*, *ASPC* 384, p.145
Kasting, J. F. & Grinspoon, D. H. 1991, in *The Sun in Time*, Univ. Arizona Press, p.447
Kochukhov, O., Makaganiuk, V., & Piskunov, N. 2010, *A&A* 524, A5
Kochukhov, O., Makaganiuk, V., Piskunov, N., *et al.* 2011, *ApJ* 732, L19
Konstantinova-Antova, R., Aurire, M., Iliev, I. Kh., *et al.* 2008, *A&A* 480, 475
Konstantinova-Antova, R., Auriére, M., Schröder, K.-P., & Petit, P. 2009, in *Cosmic Magnetic Fields: From Planets, to Stars and Galaxies*, K. G. Strassmeier, A. G. Kosovichev, & J. E. Beckman (eds.), IAU Symp. 259, CUP, p. 433
Konstantinova-Antova, R., Auriére, M., Petit, P., Charbonnel, C., Tsvetkova, S., Lébre, A., & Bogdanovski, R. 2012, *A&A* 541, A44
Küker, M. & Rüdiger, G. 1999, *A&A* 346, 922
Mestel, L. 2001, in *Magnetic Fields across the H-R Diagram*, *ASPC* 248, p.3
Martínez González, M. J., Asensio Ramos, A., Carroll, T. A., *et al.* 2008, *A&A* 486, 637
Mathys, G. & Solanki, S. K., 1989, *A&A* 208, 189
Petit, P., Auriére, M., Konstantinova-Antova, R., Morgenthaler, A., Perrin, G., Roudier, T., & Donati, J.-F. 2013, in *The Environments of the Sun and the Stars*, Lecture Notes in Physics, Volume 857, Springer Verlag, p.231
Ramírez Vélez, J. C., Semel, M., Stift, M., Martínez González, M. J., Petit, P., & Dunstone, N. 2010, *A&A* 512, A6
Reiners, A. & Basri, G. 2006, *ApJ* 644, 497
Rice, J. B. & Strassmeier, K. G. 2000, *A&AS* 147, 151
Rice, J. B., Strassmeier, K. G., & Kopf, M. 2011, *ApJ* 728, 69
Rüedi, I., Solanki, S. H., Mathys, G., & Saar, S. H. 1997, *A&A* 318, 429
Saar, S. H., 1988, *ApJ* 324, 441
Semel, M., Ramírez Vélez, J. C., Martínez González, M. J., *et al.* 2009, *A&A* 504, 1003
Sennhauser, C. & Berdyugina, S. V. 2010, *A&A* 522, A57
Sennhauser, C. & Berdyugina, S. V. 2011, *A&A* 529, A100
Shkolnik, E., Bohlender, D. A., Walker, G. A. H., & Collier Cameron, A. 2008, *ApJ* 676, 628

Skelly, M. B., Donati, J.-F., Bouvier, J., *et al.* 2010, *MNRAS*, 403, 159
Skumanich, A. 1972, *ApJ* 171, 565
Spada, F., Li, L. H., Sofia, S., & Ventura, P. 2012, in *Advances in computational astrophysics: methods, tools, and outcome*, *ASPC* 453, p. 395
Strassmeier, K. G. 2009, *A&A* Rev. 17, 251
Strassmeier, K. G. 2011, in *Advances in Plasma Astrophysics*, A. Bonanno *et al.* (eds.), IAU Symp. 274, CUP, p. 274
Strassmeier, K. G., Carroll, T. A., Weber, M., *et al.* 2011, *A&A* 535, A98
Stenflo, J. O. & Lindegren, L. 1977, *A&A* 59, 367
Valenti, J. A., Marcy, G. W., & Basri, G. 1995, *ApJ* 439, 939
Wallace, L., *et al.* 1998, *An Atlas of the Sunspot Umbral Spectrum in the Red and IR from 8900 to 15050 cm*$^{-1}$, NSO Rechn. rep. 98-002
Wood, B. E., *et al.* 2002, *ApJ* 574, 412